

Implicit Neural Representation of Waveform Measurements in Power Systems Waveform Data Analysis

Narges Ehsani, *Student Member, IEEE*, Vishwanath Saragadam, and Hamed Mohsenian-Rad, *Fellow, IEEE*

Abstract—There is currently a paradigm shift in several power system monitoring applications, such as incipient fault detection and monitoring inverter-based resources, to transition from traditional phasor analytics to more informative waveform analytics. This paper contributes to this transition by developing a novel approach to modeling voltage and current waveform measurements using implicit neural representations (INRs). INRs are continuous function approximators that are recently used in vision and signal processing. The proposed INR models are specifically designed to meet the requirements of waveform analytics in power systems, such as by using sinusoidal activation functions that capture the periodic nature of voltage and current waveforms. We also propose extended models that can efficiently represent correlated waveforms, such as three-phase waveforms and synchro-waveforms. Real-world case studies demonstrate the effectiveness of the proposed INR models in terms of accuracy ($<1\text{-}2\%$ MSE) and model size ($4\text{-}6\times$ compression). We also investigate the application of INR models in oscillation monitoring, for single mode oscillations and dual mode modulated oscillations.

Keywords: Waveform measurements, waveform analytics, implicit neural representation, sinusoidal activation, model size, three-phase measurements, synchro-waveform measurements.

I. INTRODUCTION

A. Waveform Analytics: A New Big Data Challenge

Waveforms are the most authentic and granular representation of voltage and current in power systems. Nevertheless, the traditional approach in power system monitoring has been to measure RMS values, phasors, or other filtered/processed representations of voltage and current; which results in losing some important details that are only visible in waveforms.

However, with the recent advancements in power system sensor technologies, including the advent of synchro-waveforms, and also because of the increasing complexity in power system operation caused by the high-penetration of inverter-based resources (IBRs), there is now a growing interest in conducting analysis and inference directly on waveform measurements; e.g., see the detailed discussions in [1]–[3].

Waveform data are obtained from waveform measurement units (WMUs), through event-triggered waveform capture or continuous streaming of waveform measurements [4, Ch 4]. The latter is similar to how phasor measurements are streamed by phasor measurement units (PMUs). However, WMUs report data at a much higher rate than PMUs. For example, each three-phase WMU reports 3,981,312,000 voltage readings per day (at a sampling rate of 256 samples per cycle), which can exceed one gigabyte of data per day per sensor [2], [5].

Collecting data at such high reporting rate creates a new challenge in big data analytics in power systems, moving beyond the existing big data analytics practice for traditional measurements such as from smart meters and PMUs.

B. Approach and Contributions

We seek to address some of these challenges by developing a novel approach to model waveform (and synchro-waveform) measurements. We propose to utilize the latest advancements in the field of implicit neural representation (INR). INRs are continuous function approximators based on multilayer perceptrons (MLPs). Since their first widespread usage in novel view synthesis in graphics [6], INRs have been quickly adopted in all fields of vision and signal processing, including rendering [7], medical imaging [8], and virtual reality [9].

The main contributions in this paper are as follows:

- To the best of our knowledge, this is the first study to develop INR models for waveforms in power systems. The proposed INR models are designed to meet the requirements in this new application domain, such as by using sinusoidal activation functions [10] that can capture the inherently periodic nature of voltage and current waveforms.
- The INR models with single and double hidden layers are analyzed. We show that a single hidden layer INR resembles a Fourier transform and hence cannot capture transient distortions. In contrast, we show that a double hidden layer INR does capture these complexities. This enables an approximately $3\times$ increase in accuracy for the same number of parameters as a single hidden layer INR.
- Unlike classical signal representations, INRs enable representing correlated signals with a single model. We hence extend our INR model to enhance efficiency in modeling correlated waveforms, such as among three phases, among synchro-waveforms, and between voltage and current. Experiments on real-data demonstrate that such an approach is highly advantageous in modeling sub-cycle transients that are otherwise difficult to model with separate INRs.
- Real-world case studies provide detailed sensitivity analysis and confirm the performance of the proposed INR models, both in terms of model accuracy and model size. The direct application of the INR models is investigated in analyzing two types of oscillatory events, namely single mode oscillations and dual mode modulated oscillations.

C. Related Literature

In power systems, research on INRs is still emerging, with limited studies exploring its potential. In [11], INRs are used for power system dynamic simulations. In [12], [13], INRs are used in optimal power flow analysis. In [14], INRs are utilized for load forecasting. While these studies demonstrate INR's potential in power systems, they highly differ from the focus of our research. Here, we leverage INRs not for optimization or solving partial differential equations, but to compactly represent high-resolution power system waveforms.

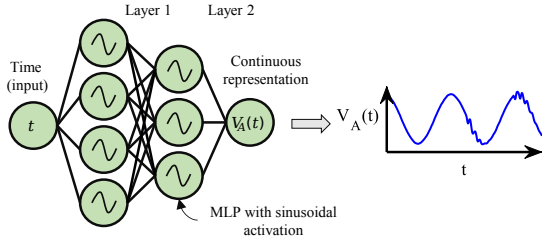


Fig. 1. The proposed INR architecture to model a single time-series of waveform measurements. The MLP has two hidden layers. The activation functions at all neurons in both hidden layers are sinusoidal functions.

The analysis in this paper also falls under the growing literature on waveform data analytics in power systems. The advent of synchro-waveform technology has given a recent boost to this field, with applications, such as for fault location identification [15], wildfire monitoring [16], oscillation monitoring [17], and dynamic modeling of IBRs [18].

The scope of this paper also has some partial overlap with the literature on data compression, such as in [19] for loss-less compression, often with focus on generic data compression techniques, or in [20] for lossy compression, often with focus on signal processing, such as Fourier and Wavelet transform. Although our proposed INR models can significantly compress the waveform data, they are not designed for data compression, but rather to provide a systematic way to model waveforms.

II. INR MODELING OF WAVEFORM MEASUREMENTS WITH SINGLE OR DOUBLE HIDDEN LAYERS

The overall architecture of the first proposed INR model is shown in Fig. 1. The input to the model is time t . The output is waveform $x(t)$, such as the time-series of voltage waveform measurements at Phase A, denoted by $v_A(t)$. The nonlinear activation function $\sigma(\cdot)$ plays a key role in the representation capacity of the INR model. In this paper, given the dominantly sinusoidal nature of the waveform measurements in power systems, we use $\sigma(\cdot) = \sin(\cdot)$. Sinusoidal activation functions are proven to provide significantly higher representation accuracy than ReLU, in particular for signals with periodic nature [10].

A. Single Hidden Layer INR

Suppose the INR model has only one hidden layer. Let a_1, b_1 and a_2, b_2 be the weights of the first layer and the second layer, respectively. We can obtain the output signal as

$$x(t) = \sum_{i=1}^h a_{2,i} \sin(a_{1,i}t + b_{1,i}) + b_2, \quad (1)$$

where h denotes the number of neurons in the hidden layer. The number of parameters in the INR model in (1) is:

$$2h + h + 1 = 3h + 1. \quad (2)$$

The formulation in (1) can be interpreted as a Fourier transform, where for each $i = 1, \dots, h$, parameter $a_{1,i}$ acts as harmonic frequency, $a_{2,i}$ acts as harmonic magnitude, and $b_{1,i}$ acts as harmonic phase angle. Therefore, the INR model with one hidden layer is comparable with the *phasor representation* of the waveform measurements. However, unlike phasors,

which focus primarily on the fundamental frequency of the power system, the model in (1) is *not* biased on any particular frequency. All the parameters are rather *trained* by a stochastic gradient descent approach. Despite this advantage, an INR with a single hidden layer cannot significantly improve the model accuracy compared to Fourier transform; because the formulation in (1) is still very similar to Fourier representation.

B. Double Hidden Layer INR

Next, suppose the INR model has two hidden layers. This is the same setup as in Fig. 1. Suppose the number of neurons in the first hidden layer and in the second hidden layer are h_1 and h_2 , respectively. Let a_1, b_1 and a_2, b_2 and a_3, b_3 be the weights of the first layer and the second layer and the third layer, respectively. We can obtain the output signal as

$$x(t) = \sum_{j=1}^{h_2} a_{3,j} \sin \left(\sum_{i=1}^{h_1} a_{2,i,j} \sin(a_{1,i}t + b_{1,i}) + b_{2,i} \right) + b_3. \quad (3)$$

The model in (3) does no longer resemble Fourier transform. Intuitively, the second hidden layer introduces higher spectral diversity, which enables a richer representation in (3) than in (1). Indeed, as explained in [21], INRs with two or more hidden layers provide a larger convergence of the frequency space than INRs with only one hidden layer. Since voltage and current waveform measurements in power systems have several higher harmonics and transient modes, there is great potential to leverage INRs based on the architecture in Fig. 1, to represent waveform measurements in power systems.

The number of parameters in the INR model in (3) is:

$$2h_1 + h_1h_2 + 2h_2 + 1. \quad (4)$$

As we will see next, this increase in parameter count dramatically increases representation accuracy of the waveforms.

C. Initial Case Study

Fig. 2 provides an example to derive INR representations for a real-world voltage waveform measurement that contains a sub-cycle oscillatory event. The raw waveform measurements capture 62 cycles, with two event cycles in the middle. Here, we only show the portion of the waveform that contains event.

In Fig. 2(a), the INR model has one hidden layer. The number of parameters is $1663 = 3 \times 554 + 1$, where $h = 554$. The Mean Squared Error (MSE) is 2.40%, which is calculated between the raw waveform measurement (blue) and the reconstructed waveform (red) using the model in (1). The MSE is calculated across the entire 62 cycles of the waveform measurements. Although this model can effectively approximate the steady-state signal, resembling the Fourier series, it lacks the capability to capture the more complex behavior in the transient component of the signal.

In Fig. 2(b), the INR model has two hidden layers, with $1661 = 2 \times 30 + 30 \times 50 + 2 \times 50 + 1$ parameters, where $h_1 = 30$ and $h_2 = 50$. Thus, the number of parameters in the two-layer INR in Fig. 2(b) is equal to the number of parameters in the one-layer INR in Fig. 2(a). However, the MSE in the two-layer model is 0.82%, which is drastically less than the MSE of 2.40% for the equal-sized INR model with one hidden layer.

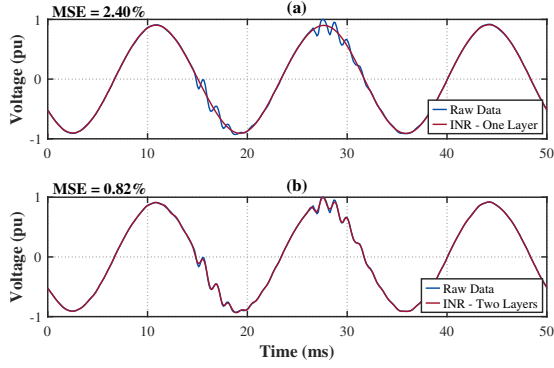


Fig. 2. Model accuracy in reconstructing a real-world voltage waveform measurement with a sub-cycle oscillatory event: (a) using the INR model with single hidden layer; (b) using the INR model with double hidden layers. The two INR models in this example have equal number of parameters.

We also evaluated the impact of using ReLU as an alternative to sine activation. The results showed that an INR model of the same size and architecture but with ReLU activation performed poorly, with an MSE of 18.88%. Accuracy was particularly low during steady-state behavior, as ReLU struggles to capture the waveform's periodic nature. Performance was also poor during transients, with an MSE of 1.56% for ReLU compared to only 0.48% for sine activation. Thus, the sinusoidal activation function clearly outperforms ReLU.

III. EXTENDED MODEL TO ENHANCE EFFICIENCY IN THREE-PHASE WAVEFORMS AND SYNCHRO-WAVEFORMS

The waveform measurements in power systems are often correlated. Correlation could exist among different waveforms, including voltages across three phases, voltages across multiple locations, and voltage and current waveforms at a given location. Such correlations may help reduce the size of the INR models. For instance, suppose we seek to model voltage waveform measurements on Phase A, Phase B, and Phase C. The waveform measurements are denoted by $v_A(t)$, $v_B(t)$, and $v_C(t)$, respectively. We have two options to derive the models:

- Develop *three separate* INR models based on Fig. 1.
- Develop *one combined* INR model based on Fig. 3.

The first option simply repeats the INR architecture in Fig. 1 three times, *once for each phase*. The number of parameters would be three times the number of parameters for one phase.

$$3 \times (2h_1 + h_1h_2 + 2h_2 + 1) \quad (5)$$

In the second option, we use *one* INR model with *three* outputs, one for each phase. In this new architecture, the two hidden layers are *shared* between the three outputs; as shown in Fig. 3. The number of parameters in this option is:

$$2h_1 + h_1h_2 + h_2 + 3 \times (h_2 + 1). \quad (6)$$

This results in significantly fewer parameters than in (5).

We can similarly apply the above approach to other cases with correlated measurements, including synchro-waveforms. For example, suppose we need to model the *time-synchronized* voltage measurements on the same phase but at five different locations. One option is to develop *five separate* INR models based on Fig. 1. The other option is to develop *one combined* INR model based on the architecture in Fig. 3, with five (instead of three) neurons in its output layer.

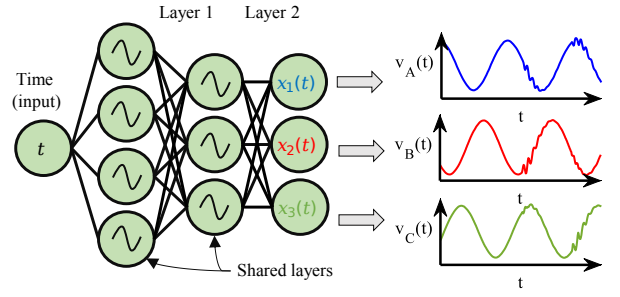


Fig. 3. The proposed model to enhance efficiency in modeling three-phase waveform measurements. A similar extension can help improve model efficiency when it comes to synchronized waveform measurements.

IV. ADDITIONAL REAL-WORLD CASE STUDIES

A. Modeling Diverse Waveform Signatures

Fig. 4 shows examples of real-world waveform measurements, including raw data (blue) and reconstructed waveforms (red) based on INR with $h_1 = h_2 = 50$. The measurements are obtained from a three-phase SEL 735 power quality sensor at 480V (line-to-line). The sampling rate of the waveform measurements is 128 samples per cycle, i.e., $128 \times 60 = 7680$ samples per second. Each waveform capture includes 62 cycles of waveform measurements, centered around the start of the event. The event signatures are diverse. They include both voltage waveforms, in Figs. 4(a)-(e), and current waveforms, in Figs. 4(f)-(i). The MSE varies from 0.77% to 2.85%.

B. Sensitivity Analysis: Number of INR Parameters

Fig. 5 provides a detailed sensitivity analysis with regards to the number of neurons in the first and second hidden layers, denoted by h_1 and h_2 , respectively. The results in Fig. 5(a) and (b) provide the MSE in modeling *voltage* and *current* waveforms, respectively. The results in Fig. 5(c) provide the corresponding model sizes, which are the same for both voltage and current waveform for the same choices of h_1 and h_2 . Each point in any curve in Figs. 5(a) and (b) is the average of $30 \times 10 = 300$ values, from 30 distinct waveform signatures and 10 runs of INR model training for each event signature. We can make several important observations based on the results in Fig. 5. First, there is a clear trade-off between the accuracy and the size of the model. Increasing both h_1 and h_2 can improve model accuracy but increase the model size. Second, increasing h_2 appears to help more than increasing h_1 in order to improve model accuracy. Third, whether we increase h_1 or h_2 , the gain in model accuracy demonstrates gradual saturation. Fourth, the model accuracy is clearly higher for voltage waveforms than current waveforms. This is because, in practice, current waveforms are often more volatile and distorted than voltage waveforms, as we saw in Fig. 4.

The computation time for training an INR model depends on the size of the model. The smallest INR model with $h_1 = 10$ and $h_2 = 10$ takes 3.63 seconds to train. The largest INR model with $h_1 = 50$ and $h_2 = 70$ takes 7.70 seconds to train. Training is done on Google Cloud Platform (GCP) using a Tesla T4 GPU with 15 GB of memory and 28 GB RAM.

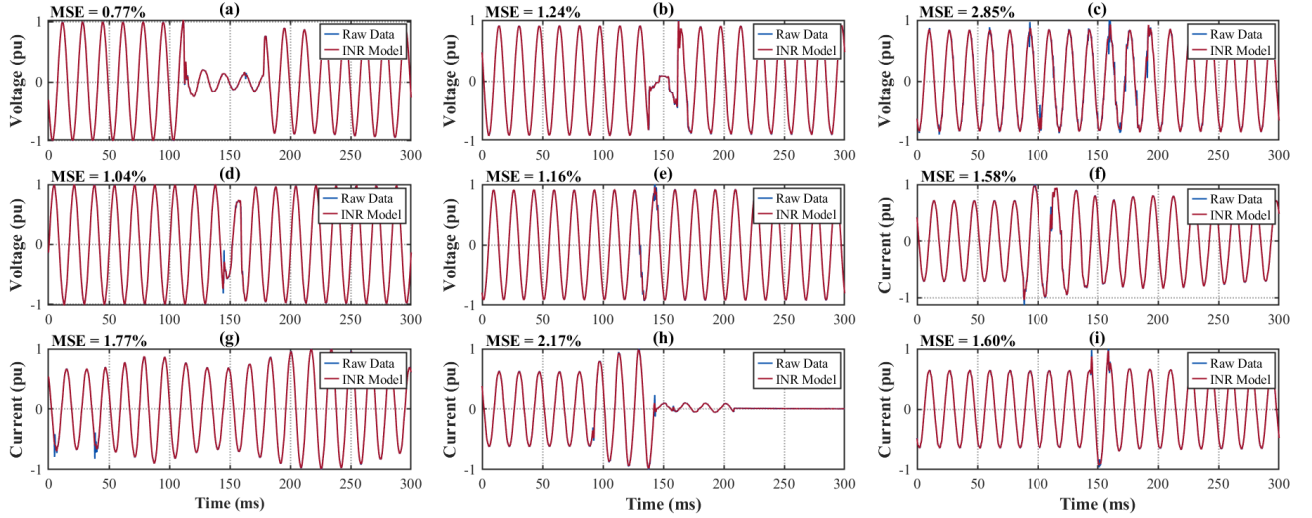


Fig. 4. Various waveform event signatures. Each example shows the raw waveform measurements, the corresponding reconstructed waveforms from an INR model with double hidden layers, and the corresponding MSE: (a)-(e) event signatures in voltage waveforms; (f)-(i) event signatures in current waveforms.

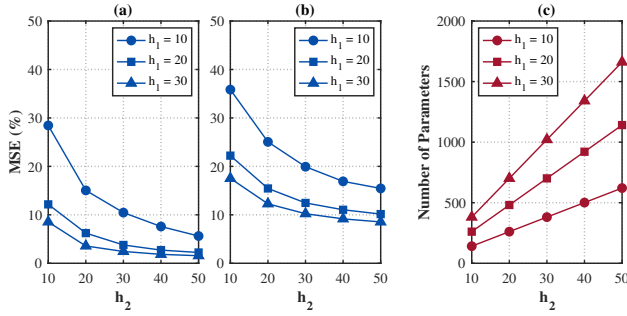


Fig. 5. Sensitivity analysis of the INR models to the number of neurons in each layer, namely h_1 and h_2 : (a) The MSE in modeling voltage waveforms; (b) The MSE in modeling current waveforms; (c) The size of the model.

C. Three Separate versus One Combined INR Model

Recall that we have two options to model three-phase waveform measurements: using three separate models as in Fig. 1 or one combined model as in Fig. 3. Fig. 6 provides a comparison between these two options. The MSE is obtained for each approach for a varying number of parameters. Each point represents the average of $3 \times 30 \times 10 = 900$ experiments, calculated from three phases of 30 distinct waveform signatures, and 10 runs of INR model training for each event. The blue points correspond to the INR model in Fig. 1, where the average output of three separate models is used. The red points correspond to the combined INR model in Fig. 3.

The results in Fig. 6(a) are for the INR models of the voltage waveform measurements, and the results in Fig. 6(b) are for the INR models of the current waveform measurements.

D. Application in Analysis of Waveform Oscillations

Lastly, we use the INR models in the analysis of real-world waveform oscillations. We study two types of oscillatory behavior, that have fundamentally different characteristics:

- Single mode oscillations, where the frequency of the dominant mode of oscillation is denoted by f_{dominant} .
- Dual mode *modulated* oscillations, where the oscillations occur at a pair of *sideband* frequencies $60 \text{ Hz} \pm f_{\text{sideband}}$.

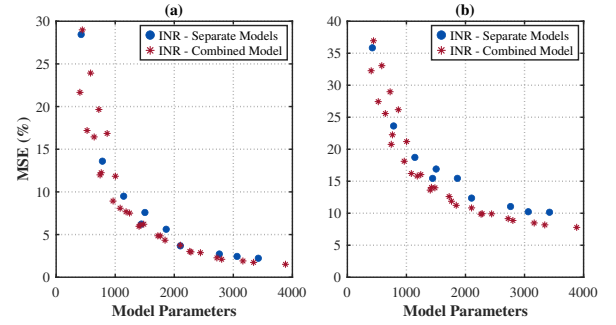


Fig. 6. Comparing the performance of three separate INR models in Fig. 1 versus one combined INR model in Fig. 3 in modeling three-phase waveform measurements. The MSE for each model is averaged over three phases and across several runs: (a) Average MSE for voltage waveforms across three phases; (b) Average MSE for current waveforms across three phases.

Both analysis require examining the *frequency spectrum* of the waveforms. Thus, we compare the frequency spectrum from the raw data, as well as the INR output, using Discrete Fourier Transform (DFT). The analysis is done on all phases. The results on Phase A are shown in Fig. 7. The raw data are *differential waveforms*, which are the extracted superimposed signature of the event on the normal waveform [4, Section 4.2.5]. Each row shows the waveforms in time domain on the left side, and the derived frequency spectrum on the right side.

The results in Figs. 7(a)-(d) for the INR model in Fig. 1, where three separate INR models are obtained for the three phases. The number of parameters in the INR model across all phases is 8103. The results in Figs. 7(e)-(h) for the INR model in Fig. 3, where a combined INR model is obtained for all three phases. The number of parameters in the INR model for all phases is 5503. The total number of parameters in the raw data for all phases in each case study is 23,808, thus achieving $4 - 6 \times$ compression with INR models.

Fig. 7(a, b, e, f) show the time and frequency content of a single-mode oscillatory event. Both separate and combined INRs accurately capture the dominant frequency f_{dominant} at 900 Hz, consistent with the raw data. Importantly, a combined INR represents the spectrum more accurately, with fewer pa-

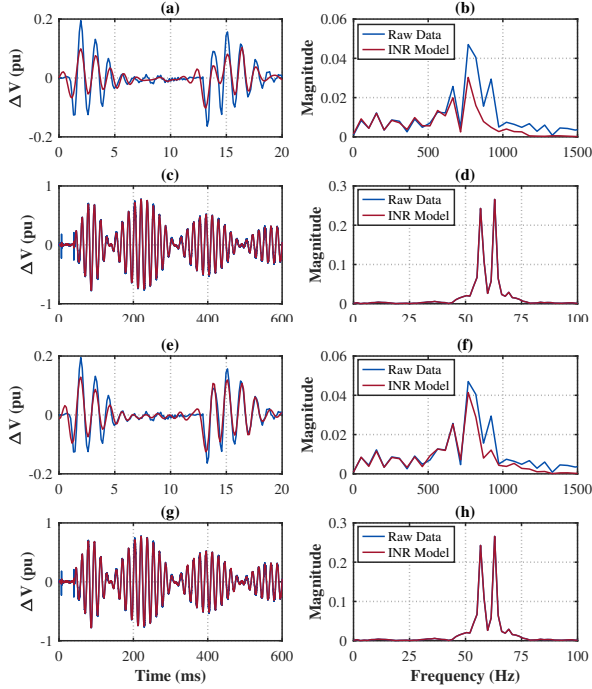


Fig. 7. Analysis of the frequency spectrum (in the right column) for two types of oscillations and two types of methods: (a)(b) single mode oscillation based on separate INRs; (c)(d) dual mode modulated oscillation based on separate INRs; (e)(f) single mode oscillation based on a combined INR; and (g)(h) dual mode modulated oscillation based on a combined INR.

rameters, enabling a more parameter-efficient representation.

Figs. 7(c, d, g, h) visualize the results for dual mode modulated oscillatory event. Both separate and combined INRs accurately model the spectra, with clear peaks at the two side band frequencies $\pm f_{\text{sideband}}$ around 60 Hz. Importantly, the combined INR enables higher accuracy with fewer parameters.

V. CONCLUSIONS AND FUTURE WORK

INR is shown to be a powerful method to model voltage and current waveform measurements in power systems. A single hidden layer INR resembles a Fourier transform and hence cannot capture transient distortions. In contrast, a double hidden layer INR provides a novel foundation to capture these complexities in power systems waveforms. In most scenarios, this enables an approximately $3\times$ increase in accuracy for the same number of parameters as a single hidden layer INR.

The proposed INR models are modified to model correlated waveform measurements with significantly fewer parameters, such as in simultaneously modeling voltage on all three phases.

Detailed sensitivity analysis was conducted based on real-world data to identify the importance of parameters, as well as to demonstrate the performance of the proposed INR models in working with both voltage and current waveform measurements during various events in power systems.

Importantly, the proposed INR models demonstrated high accuracy in modeling the key waveform characteristics not only in time domain but also in frequency domain, providing a direct application in any event characterization tasks.

This study can be extended in multiple directions. While our analysis considers up to two hidden layers in the INR architecture, exploring deeper networks and alternative architectures

may further enhance model accuracy. The robustness of INR models could also be assessed more extensively under a wider range of operating conditions, including varying noise levels and diverse event signatures. A more comprehensive comparison with state-of-the-art waveform modeling techniques can further clarify the advantages and limitations of INR models. Future work may also focus on integrating INR models into power systems monitoring and operation use cases, to support both off-line and on-line monitoring applications.

REFERENCES

- [1] A. Silverstein and J. Follum, "High-resolution time-synchronized grid monitoring devices," North American Synchrophasor Initiative Technical Report NASPI-2020-TR-004, Mar. 2020.
- [2] H. Mohsenian-Rad and W. Xu, "Synchro-waveforms: A window to the future of power systems data analytics," *IEEE Power and Energy Magazine* 21, vol. 21, no. 5, pp. 68–77, Sep 2023.
- [3] W. Xu, *et al.*, "Synchronized waveforms – a frontier of data-based power system and apparatus monitoring, protection, and control," *IEEE Trans. on Power Delivery*, vol. 37, no. 1, pp. 3–17, 2022.
- [4] H. Mohsenian-Rad, *Smart Grid Sensors: Principles and Applications*. Cambridge University Press, United Kingdom, Apr. 2022.
- [5] N. Ehsani, *et al.*, "Sub-cycle event detection and characterization in continuous streaming of synchro-waveforms: An experiment based on gridsweep measurements," in *Proc. of the IEEE North American Power Symposium*, Asheville, NC, Oct 2023.
- [6] B. Mildenhall, *et al.*, "Nerf: Representing scenes as neural radiance fields for view synthesis," in *IEEE European Conf. Computer Vision*, 2020.
- [7] A. Kuznetsov, *et al.*, "NeuMIP: Multi-resolution neural materials," *ACM Trans. Graphics*, vol. 40, no. 4, pp. 1–13, 2021.
- [8] Y. Wang, Y. Long, S. H. Fan, and Q. Dou, "Neural rendering for stereo 3d reconstruction of deformable tissues in robotic surgery," in *Intl. Conf. Medical Image Computing and Computer-Assisted Intervention*, 2022.
- [9] N. Deng, *et al.*, "Fov-nerf: Foveated neural radiance fields for virtual reality," *IEEE Trans. Visualization and Computer Graphics*, vol. 28, no. 11, pp. 3854–3864, 2022.
- [10] V. Sitzmann, *et al.*, "Implicit neural representations with periodic activation functions," *Adv. Neural Info. Processing Systems*, 2020.
- [11] M. Bossart, *et al.*, "Acceleration of power system dynamic simulations using a deep equilibrium layer and neural ode surrogate," *arXiv preprint arXiv:2405.06827*, 2024.
- [12] K. D. Smith, F. Seccamonte, A. Swami, and F. Bullo, "Physics-informed implicit representations of equilibrium network flows," in *Advances in Neural Information Processing Systems*, vol. 35, 2022, pp. 7211–7221.
- [13] P. Donti, A. Agarwal, N. V. Bedmutha, L. Pileggi, and J. Z. Kolter, "Adversarially robust learning for security-constrained optimal power flow," in *Advances in Neural Information Processing Systems*, vol. 34. Curran Associates, Inc., 2021, pp. 28 677–28 689.
- [14] Y. Xu, S. Mao, L. Pang, and J. Zhu, "Advanced energy forecasting and managing methods based on deep learning and optimization algorithm for carbon neutral," *SSRN Electronic Journal*, available at SSRN: <http://dx.doi.org/10.2139/ssrn.4778865>.
- [15] I. Khan, H. Sun, K. Kim, J. Guo, and D. Nikovski, "Combined detection and localization model for high impedance fault under noisy condition," in *Proc. of the IEEE PES General Meeting*, Orlando, FL, Jul. 2023.
- [16] H. Mohsenian-Rad, A. Shahsavari, and M. Majidi, "Analysis of power quality events for wildfire monitoring: Lessons learned from a california wildfire," in *Proc. of the IEEE PES ISGT*, San Juan, Puerto Rico, 2023.
- [17] T. Zaman, *et al.*, "Multimode synchronous resonance detection in converters dominated power system using synchro-waveforms," in *Proc. of the Int. Conference on Electricity Distribution*, Rome, Italy, Jun 2023.
- [18] F. Ahmadi-Gorjaji and H. Mohsenian-Rad, "Data-driven models for sub-cycle dynamic response of inverter-based resources using wmu measurements," *IEEE Trans. on Smart Grid*, pp. 4125–4128, Sep 2023.
- [19] S. Blair and J. Costello, "Slipstream: High-performance lossless compression for streaming synchronized waveform monitoring data," in *Proc. of the IEEE PES SGSM Conference*, Split, Croatia, May 2022.
- [20] X. Wang, Y. Liu, and L. Tong, "Adaptive subband compression for streaming of continuous point-on-wave and pmu data," *IEEE Transactions on Power Systems*, vol. 36, no. 6, pp. 5612–5621, 2021.
- [21] T. M. Roddenberry, V. Saragadam, M. V. de Hoop, and R. G. Baraniuk, "Implicit neural representations and the algebra of complex wavelets," *arXiv preprint arXiv:2310.00545*, 2023.